The Astrophysical Journal, 888:126 (10pp), 2020 January 10 https://doi.org/10.3847/1538-4357/ab5af7
© 2020. The American Astronomical Society. All rights reserved.

Chromium Isotopic Constraints on the Origin of the Ureilite Parent Body

Ke Zhu (朱柯)[1], Frédéric Moynier[1,2], Martin Schiller[3], Daniel Wielandt[3], Kirsten K. Larsen[3], Elishevah M. M. E. van Kooten[1], Jean-Alix Barrat[4], and Martin Bizzarro[3]

[1] Institut de Physique du Globe de Paris, Université de Paris, CNRS, 1 rue Jussieu, Paris F-75005, France; zhu@ipgp.fr
[2] Institut Universitaire de France, 103 boulevard Saint-Michel, Paris F-75005, France
[3] Centre for Star and Planet Formation and Natural History Museum of Denmark, Globe Institute, University of Copenhagen, Øster Voldgade 5–7, Copenhagen DK-1350, Denmark
[4] Laboratoire Géosciences Océan (UMR CNRS 6538), Université de Bretagne, Occidentale et Institut Universitaire Européen de la Mer, Place Nicolas Copernic, F-29280 Plouzané, France

Received 2019 September 30; revised 2019 November 21; accepted 2019 November 21; published 2020 January 16

Abstract

We report on the mass-independent Cr isotope compositions of 11 main group ureilites and an ureilitic trachyandesite (ALM-A). The $^{54}Cr/^{52}Cr$ ratios for main group ureilites vary from -1.06 ± 0.04 to -0.78 ± 0.05 and averaged at -0.91 ± 0.15 (2SD, $N = 18$) including the data from literature. We argue that this variation reflects primitive mantle heterogeneities within the ureilite parent body (UPB). As such, this body did not experience a global-scale magma ocean, which is consistent with heterogeneous O isotope in ureilites. Furthermore, the $\varepsilon^{54}Cr$ values, Mn/Cr ratios, C isotope ratios, Mg# values, and Fe/Mn ratios in the olivine cores of ureilites are correlated with each other, which suggests the mixing of ureilite precursors from at least two reservoirs, rather than a smelting process or the oxidation from ice melting. All the ureilite samples (including the ALM-A) fall on a well-defined ^{53}Mn–^{53}Cr isochron corresponding to a $^{53}Mn/^{55}Mn$ ratio of $(6.02 \pm 1.59) \times 10^{-6}$, which translates to an age of 4566.7 ± 1.5 Ma (within 2 Ma after calcium-aluminum-rich inclusions; CAIs) when anchored to the U-corrected Pb–Pb age for the D'Orbigny angrite. This old age indicates early partial melting on the UPB, consistent with the early accretion of the UPB (within 1 Ma after CAIs) predicted by thermal modeling. Furthermore, there is a 4∼5 Ma age difference between the external isochron in this study and internal isochron ages for the feldspathic clasts in polymict ureilites, which likely reflects an impact history during the early evolution of the UPB.

Unified Astronomy Thesaurus concepts: Astrochemistry (75); Cosmochemistry (331); Cosmochronology (332); Asteroids (72); Small solar system bodies (1469); Solar system planets (1260); Isotopic abundances (867); Nucleosynthesis (1131)

1. Introduction

Achondritic meteorites are fragments of differentiated asteroids or planetary bodies of the solar system. Ureilites are coarse-grained ultramafic (olivine–pyroxene) achondrites. They include accessory minerals of metal and sulfide associated with high abundances of carbon phases (on average 3 vol% and up to ∼7 vol%; Goodrich et al. 2015), including graphite and high-pressure diamond (Goodrich 1992; Mittlefehldt et al. 1998; Nabiei et al. 2018). According to their petrology, ureilites are further divided into main group ureilites (formerly referred to as monomict or unbrecciated ureilites; accounting for 95%) and rare polymict ureilites (or brecciated ureilites). The main group ureilites represent the mantle residues after the extraction of feldspar-rich magmas (Cohen et al. 2004; Bischoff et al. 2014; Barrat et al. 2016) and a sulfur-rich iron melt (Goodrich et al. 2004; Warren et al. 2006; Goodrich et al. 2007; Rankenburg et al. 2008; Barrat et al. 2015), whereas polymict ureilites are breccias containing fragments of main group ureilites as well as non-ureilite clasts (Goodrich et al. 2004, 2015). Unlike samples from other differentiated planetary bodies (e.g., terrestrial and lunar samples, Martian meteorites, angrites), some primitive isotopic geochemical features (e.g., O isotope heterogeneities; Greenwood et al. 2005, 2006, 2017) have been preserved in ureilites, which are considered incompatible with a magma ocean event (e.g., Goodrich 1992; Goodrich et al. 2004, 2015). Therefore, the geochemical signatures of ureilite meteorites can provide valuable information about the origin of the ureilite parent body (UPB) and the early evolution of the solar system. For instance, olivine cores from individual ureilite meteorites cover a range of Fe/Mn ratios from 3 to 57 (Goodrich 1992; Goodrich et al. 2004, 2007; Downes et al. 2008) and $\Delta^{17}O$ values (mass-independent O isotopic variations) from −2.5‰ to −0.2‰ (Clayton & Mayeda 1988, 1996; Greenwood et al. 2017). The whole rock $\Delta^{17}O$ values further correlate with both the Fe/Mn ratios and magnesium number (Mg#: molar ratio of Mg/Mg+Fe) of their olivine cores (Goodrich et al. 2004, 2015). The origin of these covariations is debated and multiple scenarios have been proposed to explain these features, including (1) a "smelting" process which causes redox reactions between C and FeO during UPB differentiation (Singletary & Grove 2003; Goodrich et al. 2007); (2) oxidation of metal due to the presence of water prior to igneous differentiation (Sanders et al. 2017); (3) inherited nebular redox variability from the precursor materials that were not homogenized during partial melting (Warren & Huber 2006; Warren 2012); (4) UPB accretion from the mixing of two different chemical and isotopic reservoirs (Barrat et al. 2017). As such, ureilite genesis still remains unclear. Understanding the origin of these geochemical correlations in ureilites is further complicated by the fact that the timing of formation and early evolution of the UPB is poorly constrained.

Chromium isotopes are well suited to address questions about planetesimal to planet formation (including the UPB) because they can provide possible genetic relationships (using solar system wide ^{54}Cr nucleosynthetic variability; Trinquier et al. 2007) as

well as age constraints (from ^{53}Mn–^{53}Cr short-lived chronometry with a half-life of 3.7 ± 0.2 Myr; Holden 1990; Lugmair & Shukolyukov 1998). The ε^{54}Cr value, which is the mass fractionation corrected deviation of the ^{54}Cr/^{52}Cr ratio from the terrestrial value in parts per 10,000, varies between bulk meteorite groups and reflects heterogeneous distribution of ^{54}Cr-rich supernova grains in the proto-solar molecular cloud material (Dauphas et al. 2010; Qin et al. 2011; Nittler et al. 2018). This is expressed by higher ε^{54}Cr values of carbonaceous chondrites (CC; Trinquier et al. 2007; Qin et al. 2010a; Yamashita et al. 2010; Petitat et al. 2011; Yamakawa & Yin 2014; Göpel et al. 2015), compared to ordinary chondrites (OC) and some differentiated meteorites (e.g., Martian meteorites, angrites, howardite–eucrite–diogenite clan, mesosiderites, acapulcoite-lodranite clan, winonaites, pallasites, and iron meteorites; Trinquier et al. 2007; Qin et al. 2010a; Li et al. 2018; Pedersen et al. 2019; Zhu et al. 2019b), whereas the enstatite chondrites (EC), the Earth, the Moon, and the aubrites have intermediate values (Trinquier et al. 2007; Qin et al. 2010a; Mougel et al. 2018).

Previous studies have demonstrated that main group ureilites and ureilitic clasts of Almahata Sitta record homogeneous but different ε^{54}Cr values: -0.91 ± 0.04 (2SE, $N = 8$) for main group ureilites and -0.77 ± 0.03 (2SE, $N = 12$) for ureilitic clasts in Almahata Sitta, respectively (Qin et al. 2010b; Yamakawa et al. 2010). Chondrites are regarded as the precursor materials for asteroids and planets (McDonough & Sun 1995), but all known chondrites (CC, OC, and EC) have ε^{54}Cr values higher than those of main group ureilites as well as of the clasts of Almahata Sitta (Qin et al. 2010b; Yamakawa et al. 2010). This also suggests that an unsampled chondritic reservoir with extreme negative ε^{54}Cr values existed in the young solar system. More importantly, the ε^{54}Cr homogeneity observed in ureilites is not consistent with their O isotope heterogeneity (Clayton & Mayeda 1988; Rumble et al. 2010; Greenwood et al. 2017). Recently, ε^{54}Cr values ranging from -1.2 to $+1.9$ were observed among different clasts in the polymict ureilite DaG319 (Van Kooten et al. 2017), and in detail, the main group clasts show ε^{54}Cr variability from -0.74 ± 0.07 to -1.28 ± 0.29, with ε^{54}Cr variations between -1.18 ± 0.11 and 1.16 ± 0.50 for the feldspathic clasts. This small-scale Cr isotopic variability suggests a possible large-scale heterogeneity within the UPB. However, polymict ureilites likely formed as regolith on ureilitic daughter bodies that reassembled in the aftermath of the catastrophic disruption of the UPB and represent only a small fraction of (<5%) the ureilites (Goodrich et al. 2015). Hence, they probably experienced contamination from materials foreign to the UPB, so the information they recorded may be not only about UPB.

A full understanding of the origin of the UPB also requires better constraints on the timing of its accretion. The long-lived and assumption-free dating systems such as U–Pb, Sm–Nd, and Rb–Sr dating cannot provide precise ages for ureilites (e.g., the most precise U–Pb age for MET 78008, without U isotope correction, is 4563 ± 6 Ma (Torigoye-Kita et al. 1995b), because the cumulates and restites are depleted in U, Th, Sm, and Rb (Goodrich et al. 1991; Torigoye-Kita et al. 1995a, 1995b). The short-lived dating systems such as the ^{26}Al–^{26}Mg and ^{53}Mn–^{53}Cr chronometers can date individual clasts (including main group and feldspathic clasts) in polymict ureilites and minerals in main group ureilites and produce internal isochron ages of ~4563 Ma (see Table 2). However, these chronological studies for clasts or minerals in individual ureilites are limited by the fact they focus on internal isochrons (that just date the cooling and crystallization for this rock). The internal isochron ages do not constrain the formation or differentiation of a whole parent body, and may reflect local rather than global events, which are usually constrained by external isochrons (e.g., Zhu et al. 2019a, 2019b). In terms of bulk sample studies (external isochrons), dating by ^{26}Al–^{26}Mg, ^{53}Mn–^{53}Cr, and ^{182}Hf–^{182}W systems were limited by the very small variations in the parent–daughter ratio that has prevented obtaining precise isochrons (Yamakawa et al. 2010; Baker et al. 2012; Budde et al. 2015).

To better constrain the timescale of differentiation using the Mn–Cr system and the degree of Cr isotopic heterogeneity of the UPB, a larger variety of ureilite samples must be studied. The Mn/Cr ratio can be modified by both volatile and magmatic processes (Moynier et al. 2007; Trinquier et al. 2008b; Zhu et al. 2019a, 2019b) because of the different geochemical behavior of Mn and Cr during these processes (Lodders 2003; Sossi et al. 2019). This makes the ^{53}Mn–^{53}Cr chronometer ($T_{1/2} = 3.7$ Myr) sensitive to major differentiation events that occurred during the first 15 Myr of the early solar system. Here, we report high-precision Cr isotope data for eleven main group ureilites and one ureilitic trachyandesite clast from the Almahata Sitta polymict ureilite (ALM-A), which has a complementary crustal composition (Bischoff et al. 2014) and also the most representative sample of the same lithology that is represented by the feldspathic clasts in polymict ureilites dated by Goodrich et al. (2010) and Van Kooten et al. (2017). We also discuss the potential relationship between the whole rock Cr isotope signatures and Mg# and Fe/Mn ratios (both correlate with Δ^{17}O values) of olivine cores in the respective samples to shed further light onto the petrogenesis of ureilites and formation of the UPB.

2. Samples and Analytical Methods

The Cr isotope compositions and Mn/Cr ratios of 11 main group ureilites and one ureilitic trachyandesite were analyzed in this study as well as two terrestrial rock standards and a whole rock sample of the CV chondrite Allende, for which previous data is already available. All selected ureilites have been previously petrographically characterized and were selected to encompass the full range of known Fe/Mn ratios in olivine cores. The bulk geochemical composition, the petrological description, and the Fe and C isotopic composition of the majority of the analyzed ureilites have been previously reported (Bischoff et al. 2014; Barrat et al. 2015, 2017) and are shown in Table 1. For each sample, around 10 mg of powders were dissolved following the protocol described in Inglis et al. (2018) using Teflon bombs and an Analab EvapoClean. The procedure involved heating a mixture of concentrated HF and HNO_3 (2:1) at 140°C for two days, and subsequent dissolution in aqua regia (concentrated HCl and HNO_3 mixture in 3:1 ratio, also at 140°C) for another two days to ensure complete digestion of fluorides and refractory phases such as chromite and spinel. Before the chemical separation of Cr, a ~5% aliquot was extracted for precise determination of the ^{55}Mn/^{52}Cr ratio by multiple collector inductively coupled plasma mass spectrometry (MC-ICP-MS) using a Thermo-Fisher Scientific Neptune Plus. The accuracy and external reproducibility of the ^{55}Mn/^{52}Cr ratio was tested using repeat measurements of PCC-1, which returned a value of 0.353 ± 0.002 (2SD, $N = 6$), which is consistent with a previously reported value of 0.370 ± 0.019 (Qin et al. 2010a). Compared the two values, the uncertainty of the ^{55}Mn/^{52}Cr can be estimated as 5%.

Table 1
Mn–Cr Data with Mg# and Fe/Mn in Olivine Cores for 19 Bulk Main Group Ureilites (Including 8 Samples in Previous Studies), One Trachyandesite (ALM-A), and Three Standards

Name	$^{55}Mn/^{52}Cr$	$\varepsilon^{53}Cr$	2se	$\varepsilon^{54}Cr$	2se	N	Olivine Cores		Yield
							Mg#	Fe/Mn	
NWA 7630	0.62	0.04	0.01	−1.01	0.04	5	79	47	91%
NWA 6056	0.72	0.19	0.05	−1.01	0.07	5	85	32	92%
NWA 5884	0.74	0.14	0.03	−0.87	0.05	6	79	48	95%
NWA 5602	0.70	0.14	0.05	−1.06	0.04	10	79	46	89%
NWA 4516	0.68	0.17	0.04	−0.86	0.06	5	81	42	84%
NWA 5555	0.78	0.20	0.06	−0.88	0.06	5	91	20	87%
NWA 4511	0.78	0.17	0.02	−0.84	0.06	5	78	51	86%
NWA 4471	0.73	0.17	0.03	−0.92	0.07	5	78	50	88%
NWA 7686	0.76	0.20	0.06	−0.92	0.08	5	91	19	91%
NWA 11368	0.77	0.25	0.04	−0.83	0.07	5	90	21	93%
NWA 2236	1.14	0.29	0.04	−0.78	0.05	5	97	7	93%
ALM-A	1.35	0.45	0.05	−0.68	0.09	12	No Olivine		84%
NWA 766[a]	0.69	0.17	0.05	−0.92	0.08		76	49	
NWA 1241[a]	0.49	0.09	0.04	−0.98	0.08		82	39	
El Gouanem[a]	0.65	0.17	0.06	−0.93	0.09		81	41	
Dhofar 132[a]	0.68	0.09	0.04	−0.97	0.09				
Dhofar 836[a]	0.73	0.19	0.06	−0.89	0.07				
NWA 2376[a]	0.75	0.16	0.04	−0.84	0.07				
DaG 340[a]	0.62	0.12	0.04	−0.98	0.10		80	44	
DaG 868[a]	0.74	0.18	0.04	−0.88	0.10				
PCC-1	0.35	0.05	0.03	0.10	0.07	5			95%
DTS-1	0.23	−0.01	0.04	0.05	0.06	6			98%
Allende	0.42	0.10	0.06	1.10	0.08	8			95%

Note. Cr isotopic data marked "a" are from Yamakawa et al. (2010), and the Mg# and Fe/Mn data in olivine cores for the ureilites are from literature data (Skirdji & Warren 2001; Singletary & Grove 2003; Ikeda 2007; Barrat et al. 2015, 2017).
[a] Cr isotopic data from Yamakawa et al. (2010).

Chromium was purified from 50% aliquots of dissolved samples, based on a procedure involving a three-step chromatographic ion-exchange purification protocol described in Zhu et al. (2019b) and Larsen et al. (2018) and using Cr pre-treatment procedures to promote appropriate Cr-speciation described in detail in Larsen et al. (2016). In detail, we used an anion chromatographic purification column to efficiently remove Fe from the remaining sample aliquot in 6M HCl, followed by elution of Cr through a cation exchange column in 0.5M HNO_3 (Bizzarro et al. 2011), and subsequent elution of Mg, Ca, Mn, and Ni in 6M HCl. Prior to sample loading on the cation exchange column, we used a Cr pre-treatment procedure involving dissolution in 10M HCl at >120°C to efficiently promote the formation of Cr(III)-Cl species, which have a low affinity for the cation exchanger and thus elute early (Trinquier et al. 2008a; Larsen et al. 2016). The third ion-exchange column step aimed at Cr purification from the potential interfering element Fe (and other high-field-strength elements Ti and V) and Na (as well as potential organics) using a small cation exchange column and 0.5M HNO_3, 1M HF, and 6M HCl as eluants (Larsen et al. 2018). Prior to sample loading onto this last column, Cr was pre-treated by exposure to 0.5M HNO_3 + 0.6% H_2O_2 at room temperature for two days to promote the formation of Cr^{3+} (Larsen et al. 2016). The total yields for this purification range from 84% to 98% (calculated by the comparison between final Cr cut and the washes from the chemistry) and chromium total chemistry blanks are smaller than 2 ng and, thus, negligible compared to the processed 5 to 30 μg of Cr. After chemistry, the final Cr solution was fluxed for 1 day in 250 μl concentrated aqua regia and concentrated HNO_3, respectively, to minimize residual organics (i.e., introduced from the cation exchange resin).

The Cr isotopic compositions of all the samples except for ALM-A were determined using the MC-ICP-MS Neptune Plus located at the Centre for Star and Planet Formation, University of Copenhagen. Detailed analytical and data reduction methods are described in Schiller et al. (2014) and Pedersen et al. (2019). Each sample was measured by sample-standard bracketing using the NIST SRM 979 Cr standard, and the sample solution with a concentration of 0.5 ∼1 ppm was introduced by A-PEX, with the ^{52}Cr signal of 20∼30 V. Each sample was measured 5–10 times, subject to the available Cr amount. The Cr isotopic composition of ALM-A was measured on the Thermal Ionization Mass Spectrometer Thermo Scientific TRITON at the Centre for Star and Planet Formation, University of Copenhagen. This sample was measured alongside the samples reported in Zhu et al. (2019b) and the related methods have been described in detail in previous studies (Van Kooten et al. 2016; 2017). The $^{53}Cr/^{52}Cr$ and $^{54}Cr/^{52}Cr$ ratios were normalized to a constant $^{50}Cr/^{52}Cr$ ratio of 0.051859 using an exponential law (Lugmair & Shukolyukov 1998). All the measured isotopic ratios are relative to NIST SRM 979 and expressed in the epsilon notations:

$$\varepsilon^{x}\mathrm{Cr} = \left(\frac{(^{x}\mathrm{Cr}/^{52}\mathrm{Cr})_{\mathrm{sample}}}{(^{x}\mathrm{Cr}/^{52}\mathrm{Cr})_{\mathrm{NIST\ SRM\ 979}}} - 1\right) \times 10000, \qquad (1)$$

with $x = 53$ or 54.

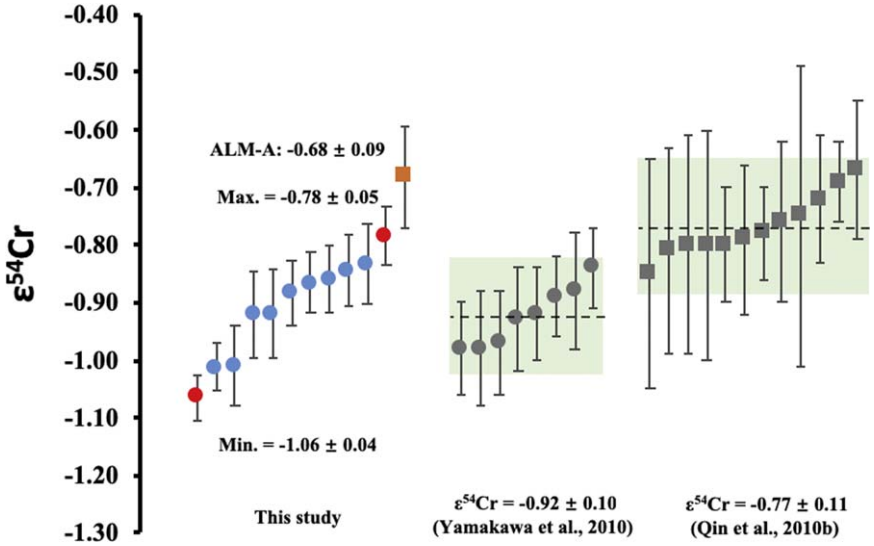

Figure 1. Comparison of ε^{54}Cr values for bulk ureilites (circles) and individual Almahatta Sitta clasts (squares) reported in different studies. The blue circles are the data from this study, which exhibit resolvable ε^{54}Cr difference between individual ureilites, whereas the gray symbols are from the literature. The two red circles indicate the maximum and minimum values. The dashed lines indicate the average ε^{54}Cr values, and green shading represents the 2SD uncertainty of the average values.

3. Results

All the Mn–Cr data for the 11 main group ureilites, the Almahata Sitta trachyandesitic clast (ALM-A), and the geological standards: DTS-1, PCC-1, and Allende are reported in Table 1, together with previously published data for another eight main group ureilites (Yamakawa et al. 2010). The ε^{53}Cr and ε^{54}Cr values for Allende, DTS-1, and PCC-1 agree well with previously published data (Shukolyukov & Lugmair 2006; Moynier et al. 2007; Trinquier et al. 2007, 2008b; Qin et al. 2010a) and have slightly better precision, providing confidence in the accuracy of our data. The ε^{54}Cr values of all the main group ureilites vary from -1.06 ± 0.04 to -0.78 ± 0.05, with an average value of -0.91 ± 0.15 (2SD, $N = 19$). A regression of the bulk ureilite ε^{53}Cr values with their respective ^{55}Mn/^{52}Cr ratios calculated with *IsoplotR* using model 1 and a Yorkfit (Vermeesch 2018) and which takes individual uncertainties (2se) into account, yields a slope of 0.558 ± 0.190 and an intercept of -0.25 ± 0.13 (MSWD = 5.1; $N = 19$). The ALM-A clast investigated in this study has the highest ^{55}Mn/^{52}Cr ratio, ε^{53}Cr, and ε^{54}Cr values (its ε^{54}Cr, -0.68 ± 0.09, is the same as that of some main group ureilites within uncertainty), and also falls on the Mn–Cr correlation line. If ALM-A is included this correlation line, the slope and intercept will change to 0.531 ± 0.140 and -0.24 ± 0.10 (MSWD = 4.9; $N = 20$; Figure 2). Notably the ε^{53}Cr (^{55}Mn/^{52}Cr) and ε^{54}Cr values appear to correlate (Figure 3(a)). Also, the Cr isotope variation broadly correlates with Mg# and Fe/Mn in olivine cores (Figures 3(c)–(f)). However, the correlation coefficients for these correlations between ε^{54}Cr and Mg# and Fe/Mn ratios in olivine cores (Figures 3(c) and (d)) are not very high, mainly because of the limited ε^{54}Cr heterogeneity in the main group ureilites.

4. Discussion

4.1. ε^{54}Cr Heterogeneity in the Mantle of UPB

Before discussing the significance of the Cr isotope data, we first consider potential cosmogenic effects that may have altered the primordial Cr isotopic composition of ureilites similar to what is observed in iron meteorites and lunar samples that have high Fe/Cr ratios and long cosmic-ray exposure (CRE) ages (Shima & Honda 1966; Qin et al. 2010a; Bonnand & Halliday 2018; Mougel et al. 2018; Liu et al. 2019). Ureilites typically have low Fe/Cr ratios (<50, molar ratio; Mittlefehldt et al. 1998), and short CRE ages (typically <50 Ma; Eugster 2003; Rai et al. 2003). Consequently, using the calculation method in Trinquier et al. (2007), the estimated contributions from galactic cosmic-rays do not exceed 0.01 epsilon for both ε^{53}Cr and ε^{54}Cr. Given that these values are significantly smaller than the analytical uncertainties, we consider CRE as a source for ε^{53}Cr and ε^{54}Cr variability not important. This conclusion is supported by the observation that angrites have similar CRE ages to ureilites and higher Fe/Cr ratio than ureilites but their Cr isotope compositions also lack any resolvable CRE effects (Zhu et al. 2019b).

Combining our ε^{54}Cr data for main group ureilites with literature data (Yamakawa et al. 2010) demonstrates that the UPB's mantle ε^{54}Cr isotopic composition is more variable than has been previously observed for bulk samples (Figure 1). This may be the result of the limited number ($N = 8$) of samples investigated by Yamakawa et al. (2010) together with the relatively large external reproducibility (~0.15 epsilon on ε^{54}Cr) in Qin et al. (2010b).

Combining all the ε^{54}Cr data for main group ureilites (including those of Yamakawa et al. 2010) result in essentially the same average ε^{54}Cr signature for ureilites (-0.91 ± 0.15; 2SD, $N = 19$) but increases the standard deviation from 0.10 to 0.15 epsilon. Given that our data is of similar or better precision than those obtained by Yamakawa et al. (2010), we interpret the larger variability to more accurately reflect preserved isotopic inhomogeneity with a ε^{54}Cr scale of ~0.3 in the mantle of the UPB.

Given this observation, we also include the ε^{54}Cr data from Qin et al. (2010b) for Almahatta Sitta ureilitic clasts and mineral separates excluding one spuriously anomalous ε^{54}Cr value (the authors thought it is likely caused by analytical artifacts) to better understand the degree of isotopic heterogeneity within the UPB material. Combining these data results in a lower ε^{54}Cr and larger standard deviation (-0.85 ± 0.20;

2SD, $N = 32$). However, the slightly higher ε^{54}Cr (-0.77 ± 0.11; 2SD, $N = 12$) for Alamahata Sitta relative to that of main group ureilites might result from the contamination of foreign materials (including CC, OC, EC, and R chondrites, which all have higher ε^{54}Cr values than main group ureilites) on the surface of UPB (Goodrich et al. 2015), and so do other polymict ureilites (Goodrich et al. 2015), which show a larger Cr isotopic heterogeneity (Van Kooten et al. 2017). In detail, the ε^{54}Cr values for different types of clasts in a polymict ureilite vary from -1.1 to $+1.9$ (Van Kooten et al. 2017). Feldspathic clasts possess ε^{54}Cr ranging from -1.2 to $+1.2$; whereas xenolithic dark clasts have very positive ε^{54}Cr values (1.55 ± 0.48; $N = 4$, 2SD), which are regarded as fragments from CC components (Van Kooten et al. 2017). Hence, the feldspathic clasts are suggested to represent impact-derived melts that reflect mixtures of ^{54}Cr-rich CC-like with ^{54}Cr-poor UPB-like material (Van Kooten et al. 2017). Since the dark and feldspathic clasts in polymict ureilites have different ε^{54}Cr origins than the main group ureilites, they cannot represent the primitive mantle of the UPB (e.g., Brearley 1992; Kita et al. 2004).

In contrast, the main group ureilites, with an average ε^{54}Cr of -0.91 ± 0.15 (2SD, $N = 18$), likely represent the initial composition of the UPB that was not contaminated by accretion of outer solar system materials. The negative ε^{54}Cr compositions recorded by main group ureilites exclude a possible relationship between ureilites and CC (which all have positive ε^{54}Cr values), which reinforces the conclusion from Yamakawa et al. (2010) and Van Kooten et al. (2017) as well as that inferred from the chemical composition (Goodrich 1999; Warren 2011; Goodrich et al. 2015) and other isotope systems, e.g., Ti, Ca, and Ni (Chen et al. 2011; Warren 2011; Schiller et al. 2018). Furthermore, all the ureilites have ε^{54}Cr values that are also lower than that of the most ^{54}Cr-poor chondrites, the OC ($\varepsilon^{54}\text{Cr} = -0.39 \pm 0.08$; 2SD, $N = 25$; Trinquier et al. 2007; Qin et al. 2010a; Pedersen et al. 2019), suggesting an unsampled chondritic reservoir with more negative ε^{54}Cr (than OC) as a source for the UPB. These very low values of ε^{54}Cr for ureilites have also been observed for other neutron-rich elements (e.g., Ti, Ca, and Ni isotopes; Chen et al. 2011; Warren 2011; Schiller et al. 2018). This suggests that the UPB accreted possibly beyond the ice line and outer asteroid belt (Yamakawa et al. 2010; Goodrich et al. 2015). Alternatively, the ε^{54}Cr variability may be temporal rather than spatial and reflect early accretion of the UPB relative to the larger bodies such as Mars and Earth (Goodrich et al. 2015, 2017; Schiller et al. 2018).

Among ureilites, both ε^{53}Cr (and Mn/Cr) and ε^{54}Cr correlate with Mg# and Fe/Mn ratios from their olivine cores (Figure 3). Furthermore, since Mg# and Fe/Mn ratios from their olivine cores have been shown to correlate with Δ^{17}O and δ^{13}C values (Clayton & Mayeda 1996; Barrat et al. 2017; Sanders et al. 2017), the ε^{53}Cr and ε^{54}Cr values should also correlated with Δ^{17}O and δ^{13}C. However, this relationship was not found among the ureilitic clasts of Almahata Sitta (Qin et al. 2010b; Rumble et al. 2010), mainly because of the large uncertainty of the data and/or some clasts were contaminated by non-ureilite material during late accretion/regolith development (Van Kooten et al. 2017). Since all the main group ureilites have variable ε^{54}Cr, the UPB could not have experienced large-degree global melting that would have homogenized the isotopic composition, which is consistent with the heterogeneous Δ^{17}O values in ureilites (Clayton & Mayeda 1988, 1996; Greenwood et al. 2017). Therefore, the variability of the Mn/Cr ratio for main group ureilites must reflect the variable composition of the precursor material instead of being solely caused by a magmatic process. The correlation between ε^{53}Cr (i.e., Mn/Cr), ε^{54}Cr, Mg#, Fe/Mn, Δ^{17}O, and δ^{13}C in main group ureilites suggests that the ureilitic precursors represent the mixing between two reservoirs, one characterized by high ε^{53}Cr, high ε^{54}Cr, high Mg#, low Fe/Mn, low Δ^{17}O, and low δ^{13}C, and the other by low ε^{53}Cr, ε^{54}Cr, and Mg#, and high Fe/Mn, Δ^{17}O, and δ^{13}C. This two-endmember mixing model for the origin of UPB is consistent with the conclusion based on C, O, and noble gas isotope variation (Barrat et al. 2017; Broadley et al. 2019). It also refutes the origin of the variable Δ^{17}O values by mixing high Δ^{17}O from ice with lower Δ^{17}O from silicates (Sanders et al. 2017), since the ice contains no chromium. Furthermore, ε^{54}Cr values (mass-independent fractionation) would not likely be altered by the "smelting" process (heating and redox reactions) as they represent primitive signatures and so the Cr isotopic data in this study refute the smelting models as well (Singletary & Grove 2003; Goodrich et al. 2007). Finally, since the variable Mg# values in ureilite olivine cores was not caused by heating process (the temperature is controlled by the depth) based on Cr isotopes, the UPB should not have the layered structure (e.g., Goodrich et al. 2004, 2007, 2015).

It should be noted that the minerals and acid leachates for an individual main group ureilite have homogeneous ε^{54}Cr values (Yamakawa et al. 2010), which indicates that individual samples experienced melt extraction and high-T equilibration, although the UPB show a global-scale ε^{54}Cr heterogeneity. This primitive melting event for ureilitic building blocks can potentially be dated by the coupled variation of ^{55}Mn/^{52}Cr and ε^{53}Cr for ureilites.

4.2. Timescale of UPB's Evolution

The ^{55}Mn/^{52}Cr ratios for the main group ureilites are also correlated with the ε^{53}Cr values (Figure 2). If this correlation line has chronological significance, its slope corresponding to a ^{53}Mn/^{55}Mn ratio of $(6.33 \pm 2.15) \times 10^{-6}$ translates into an absolute age of 4567.0 ± 1.9 Ma (within 2 Ma after calcium-aluminum-rich inclusions; CAIs; Connelly et al. 2012) when anchored to the U-corrected Pb–Pb age (4563.37 ± 0.25 Ma) for D'Orbigny (Amelin 2008; Brennecka & Wadhwa 2012) with a ^{53}Mn/^{55}Mn ratio of $(3.24 \pm 0.04) \times 10^{-6}$ (Glavin et al. 2004). The uncertainties associated with the slope of the isochron, the half-life of ^{53}Mn, the U-corrected Pb–Pb age, and the ^{53}Mn/^{55}Mn initial ratio of D'Orbigny are all propagated into the final age uncertainty. However, the ε^{54}Cr values for the main group ureilites are not homogeneous and correlate with their ^{55}Mn/^{52}Cr and ε^{53}Cr (Figures 3(a), (b)), suggesting that ureilites did not simply originate from a ε^{54}Cr isotopic homogeneous reservoir.

First, the ε^{53}Cr variation should only be due to the decay of ^{53}Mn (for sample s with low Fe/Cr and CRE ages) rather than variable distribution of nucleosynthetic products (ε^{54}Cr variation), as has already been discussed in Zhu et al. (2019a). Previous studies of meteoritic material have not been able to link ^{53}Cr isotopic anomalies to nucleosynthetic variability unrelated to the radioactive decay from ^{53}Mn. In fact, during stepwise-leaching experiments chondrites do not exhibit covariations of ε^{53}Cr and ε^{54}Cr (Trinquier et al. 2007; Petitat et al. 2011; Yamakawa & Yin 2014; Göpel et al. 2015) that

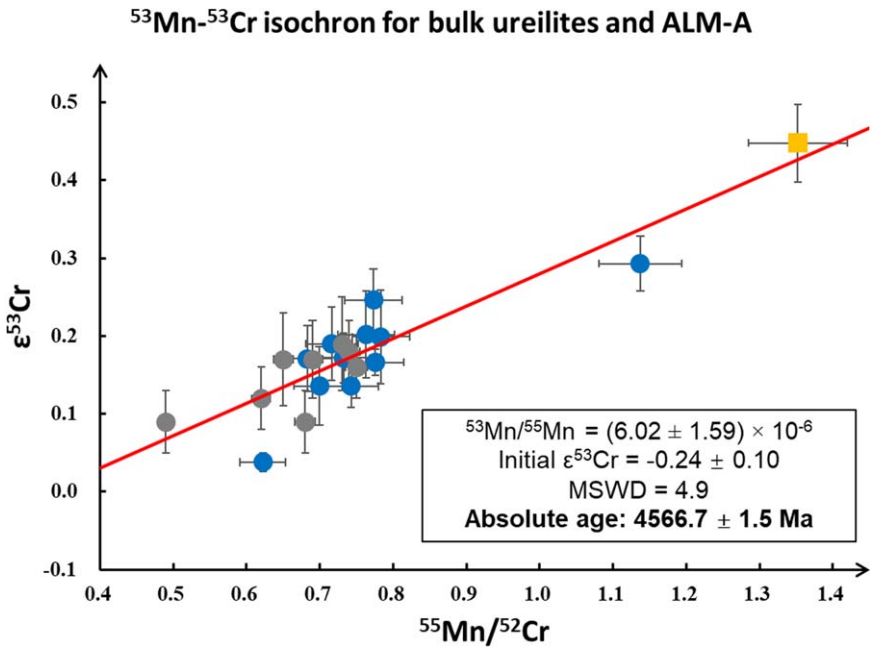

Figure 2. Mn–Cr isochron for bulk ureilites. The blue circles are ureilites in this study, while the gray circles are the data from Yamakawa et al. (2010) and the orange square is ALM-A. All uncertainties are reported as the 2σ. The ε^{53}Cr values display a positive correlation with the ^{55}Mn/^{52}Cr ratio. The slope of the line corresponds to an age of 4566.7 ± 1.5 Ma. The Mn–Cr age is relative to the U-corrected Pb–Pb age for the D'Orbigny angrite.

would hint against the existence of a carrier characterized by both ^{54}Cr and ^{53}Cr nucleosynthetic enrichments. More importantly, ^{54}Cr carrier phases detected in acid residues of the CI chondrite Orgueil show extremely high ^{54}Cr enrichments (up to 56 times the solar value), but lack corresponding resolvable ^{53}Cr anomalies (Dauphas et al. 2010; Qin et al. 2011; Nittler et al. 2018). Compared to the extreme ^{54}Cr carrier phases, the ureilites only possesses very limited ε^{54}Cr deficits, such that potential nucleosynthetic contributions to ε^{53}Cr in ureilites, if present, are likely to be insignificant. Therefore, at the current stage of our knowledge, the correlation between ε^{53}Cr and ε^{54}Cr most likely reflects primordial heterogeneity of the UPB, with two endmember compositions that are broadly characterized by a high Mn/Cr ratio and ε^{54}Cr values and low Mn/Cr ratios and ε^{54}Cr values, respectively.

Since the ε^{54}Cr signatures for the ureilites were never homogenized, the obtained Mn–Cr age cannot reflect the complete melting and differentiation of the UPB. In contrast, for Vesta (Mn–Cr age of ∼2.5 Ma after CAIs; Trinquier et al. 2008b) and the angrite parent body (Mn–Cr age of ∼4.1 Ma after CAIs; Zhu et al. 2019b), their Mn–Cr ages likely reflect global magmatic processes, since both the two asteroids have homogeneous ε^{54}Cr. It should be noted that the ε^{54}Cr values of the ureilites correlate with their respective Mn/Cr ratios and ε^{53}Cr values, so the time significance for this correlation line can be explained as the formation (separation) of the two ureilitic reservoirs suggested in Section 4.1. If true, this scenario requires that the two ureilitic reservoirs evolved with the same initial ε^{53}Cr (∼−0.28) as well as initial ^{53}Mn/^{55}Mn abundance (which is a basic assumption for short-lived chronology, and has been demonstrated; see Introduction) and formed at the same time. Then, they should penultimately fall onto the same isochron, despite being characterized by variable ε^{54}Cr signatures. Thus, the formation of the two ureilitic reservoirs must predate the mixing for ureilite precursors. The Mn/Cr fractionation between the two reservoirs can be caused by their different volatile history. On the one hand, they may have formed at variable heliocentric distances, which would result in different temperature for the formation of the two reservoirs and finally cause their Mn/Cr fractionation due to different volatility of Mn and Cr (Lodders 2003). Their potential different location is also consistent with their different ε^{54}Cr values. On the other hand, their Mn/Cr ratio variation could have arisen from different oxygen fugacity if they experienced similar conditions for temperature, because the volatility for Cr decreases with increasing oxygen fugacity, whereas the volatility for Mn and most of other elements are boosted in oxidized conditions (Sossi et al. 2019).

This age and time significance for the isochron of ureilites are similar to the Mn–Cr age of CO chondrule precursors (4567.6 ± 1.3 Ma) which also record ε^{54}Cr heterogeneity and correlation between ε^{53}Cr and ε^{54}Cr among individual chondrules (Zhu et al. 2019a). This suggests that chondrules may form the building blocks for the UPB, which is consistent with the chondrule accretion model indicating chondrules may represent the pebbles at the origin of the building blocks for the terrestrial planets (Johansen et al. 2015). However, this age of CO chondrule precursors is older than some of the last melting ages for individual chondrules (dated by U-corrected Pb–Pb chronometry; e.g., OC, CV, and CR chondrules) that can span up to 4 Ma after CAI (Connelly et al. 2012; Bizzarro et al. 2017; Bollard et al. 2017). This observation can be reconciled considering that chondrule precursors rather than chondrules may represent the building blocks for the planetesimals (Johansen et al. 2015), which can be supported by the ε^{54}Cr for chondrules in OCs, down to −0.87 ± 0.09 (Bollard et al. 2019).

It may also be possible that the precursors for other terrestrial planets, like Earth, Moon, APB, Mars, and Vesta, are also isotopically heterogeneous. However, unlike the UPB, they experienced a large-scale magma ocean that homogenized the

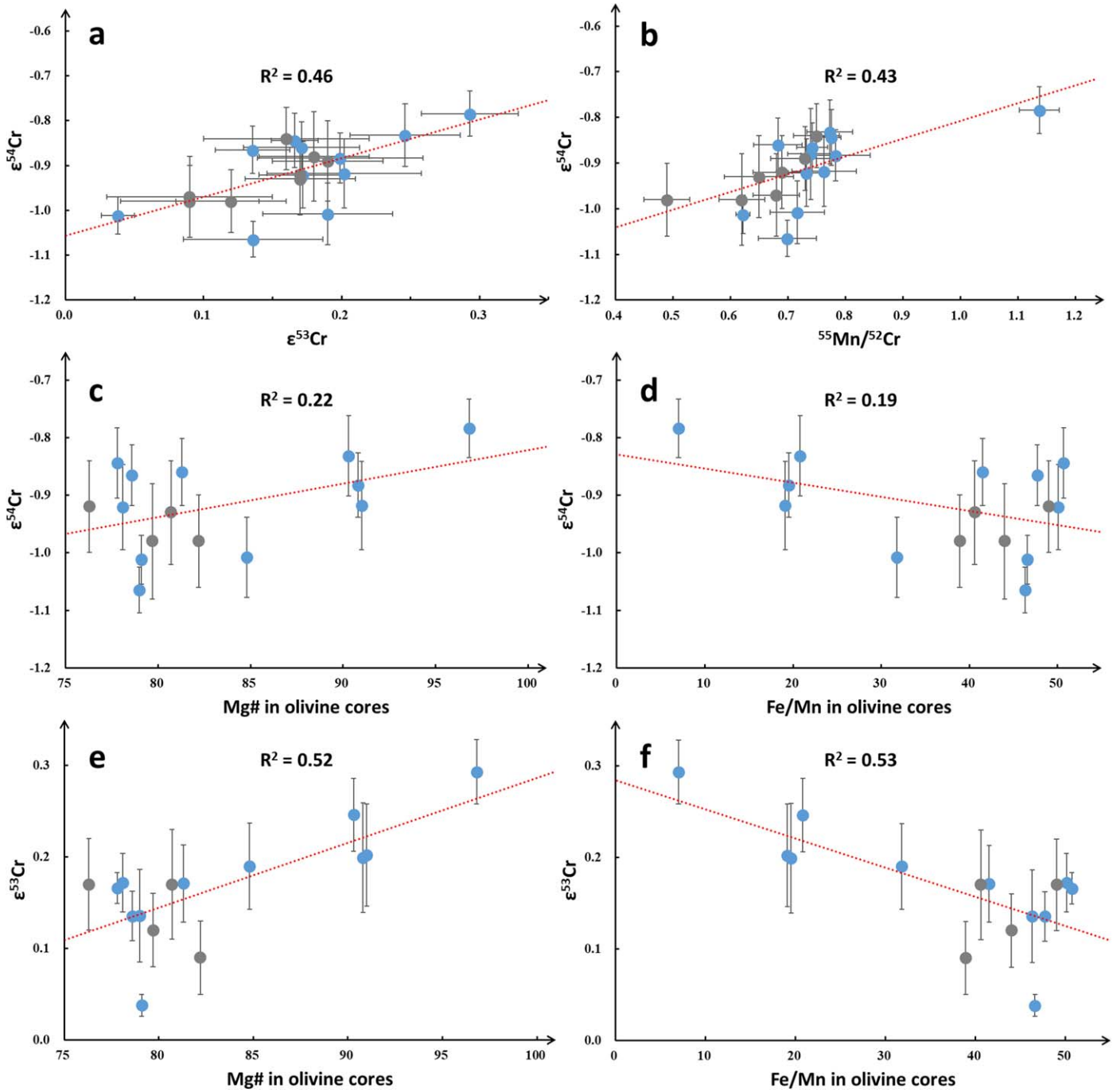

Figure 3. ε^{54}Cr vs. ε^{53}Cr (a), ^{55}Mn/^{52}Cr (b), Mg# (c), and Fe/Mn in olivine cores (d), respectively, and ε^{53}Cr vs. Mg# (e) and Fe/Mn in olivine cores (f). Also, blue points are data in this study, and gray points are from Yamakawa et al. (2010; see Table 1). Among them, ^{55}Mn/^{52}Cr, ε^{53}Cr, ε^{54}Cr, and Mg# in olivine cores are positively correlated, while all of them are negatively correlated with Fe/Mn in olivine cores. Because Mg# and Fe/Mn in olivine cores for ureilites are further correlated with the O and C isotopes, the Mn/Cr, ε^{53}Cr and ε^{54}Cr should also correlate with O and C isotopes.

potential heterogeneous isotope ratios, including Δ^{17}O, ε^{54}Cr, ε^{48}Ca, ε^{50}Ti, and ε^{62}Ni (Clayton & Mayeda 1988; Trinquier et al. 2007, 2009; Chen et al. 2011; Warren 2011; Zhang et al. 2012; Johansen et al. 2015; Greenwood et al. 2017; Schiller et al. 2018; Sossi et al. 2018; Zhu et al. 2019b, 2019c). Whereas, the reason why the UPB does not have enough heat to cause a global-scale melting is mainly because they were not large enough to preserve the heat inferred from thermal modeling (Wilson et al. 2008; Goodrich et al. 2015) and Ca isotopic evidence (Schiller et al. 2018). However, the estimated small size of UPB is inconsistent with a large UPB model suggested by the high C content in ureilites (Warren 2011), C isotope compositions (Barrat et al. 2017), and observation of high-pressure minerals in Ureilitic clasts (Nabiei et al. 2018). Another possible reason can be the ^{26}Al heterogeneity in the solar system (Larsen et al. 2011), which means the less ^{26}Al in the UPB accretion region cannot provide enough heat to a large-scale magma ocean on UPB.

It should also be noted that the ALM-A, representing a melt composition, has similar ε^{54}Cr with the main group ureilites. It also falls on this Mn–Cr correlation line, and all the main group ureilites and the ALM-A plot a very similar isochron, with

Table 2
A Review of Chronological Studies for Ureilites

Sample Type	Sample Name	Dating System	Absolute Age (Ma)	Reference
Bulk main group ureilites + ALM-A		^{53}Mn–^{53}Cr	4566.7 ± 1.5	this study
Bulk main group ureilites		^{26}Al–^{26}Mg	4566.6 ± 2.0*	[1]
Main group and Hughes type clasts	DaG 319	^{53}Mn–^{53}Cr	4567.9 ± 0.8	[2]
Feldspathic clasts	DaG 319	^{53}Mn–^{53}Cr	4564.0 ± 2.2	[2]
Feldspathic clasts	DaG 319	^{26}Al–^{26}Mg	4562.7 ± 0.3	[3]
Feldspathic clasts	DaG 319	^{26}Al–^{26}Mg	4563.4 ± 0.3	[4]
Feldspathic clasts	DaG 165	^{53}Mn–^{53}Cr	4563.1 ± 0.5	[3]
Clasts (including magnetic ones)	Almahata Sitta	^{53}Mn–^{53}Cr	4563.1 ± 1.9	[5]
Minerals and acid leachates	NWA 766	^{53}Mn–^{53}Cr	4563.6 ± 0.7	[6]
Feldspathic clasts	ALM-A	^{26}Al–^{26}Mg	4562.0 ± 0.9	[7]
Pyroxene and whole rock fractions	ALM-A	U–Pb	4562.0 ± 3.4	[8]

Note. All the ^{53}Mn–^{53}Cr and ^{26}Al–^{26}Mg ages are anchored to the absolute age for U isotope-corrected D'Orbigny with a ^{53}Mn/^{55}Mn ratio of $(3.24 \pm 0.04) \times 10^{-6}$ and a ^{26}Al/^{27}Al ratio of $(3.98 \pm 0.15) \times 10^{-7}$ (Glavin et al. 2004; Amelin 2008; Brennecka & Wadhwa 2012; Schiller et al. 2015), except the Al–Mg age for bulk main group ureilites (marked *) is a modal age.

References. [1] Baker et al. 2012, [2] Van Kooten et al. (2017), [3] Goodrich et al. (2010), [4] Kita et al. (2003), [5] Qin et al. (2010b), [6] Yamakawa et al. (2010), [7] Bischoff et al. (2014), [8] Amelin et al. (2015).

^{53}Mn/^{55}Mn ratio of $(6.02 \pm 1.59) \times 10^{-6}$, which can be translated to 4566.7 ± 1.5 Ma anchored to U-corrected D'Orbigny. Considering main group ureilites are mantle rocks and have experienced partial melting (Goodrich 1992, 1999; Goodrich & Delaney 2000; Goodrich et al. 2004; Warren 2011; Barrat et al. 2016), and Mn/Cr ratios can be effectively fractionated by magmatic process due to different compatibility for Mn and Cr (e.g., Trinquier et al. 2008b), this correlation line for all the main group ureilites and ALM-A may be an isochron recording the partial melting process that happened early on the UPB, less than 2 Ma after CAI formation. This is consistent with the ureilitic precursor age, 4567.0 ± 1.9 Ma, which is also within the first 2 Ma after CAIs, because the partial melting must predate the precursor formation. In summary, initially, the two ureilitic reservoirs formed (dated by all the main group ureilites), and then the ureilitic precursors from the two reservoirs were mixed. Next, the UPB started to accrete and experience a partial melting (and also core formation) due to its growing size, which is dated by all the main group ureilites and ALMA. However, the partial melting should be limited, because it cannot homogenize the isotopic systems discussed above, which has been predicted by thermal modeling of Wilson et al. (2008).

Since partial melting should postdate the planetary accretion, the UPB must have accreted very early, within 2 Ma after CAIs, as concluded by previous work (Wilson et al. 2008; Goodrich et al. 2015; Van Kooten et al. 2017). The early accretion of the UPB is also consistent with the thermal modeling and radiogenic ^{26}Mg deficits isotopes that predict rapid accretion of the UPB (<1 Ma after CAI; Wilson et al. 2008; Baker et al. 2012) and the very short (<1 Myr) timescales required for the accretion of asteroids (Weidenschilling 2011). As such, our Mn–Cr age further supports rapid accretion and partial melting of the UPB within 1 Ma after CAIs. However, there is only one ureilitic sample with a complementary partial melt composition, so it needs more samples to certify the partial melting age for the UPB in the future. However, both the Mn–Cr ages reported here are obviously older than the Hf-W modal age (3.3 ± 0.7 Ma after CAI) for bulk ureilites, which was interpreted as the time for silicate melt extraction on UPB (Budde et al. 2015). The reasons for the discrepancy between Mn–Cr and Hf-W ages are unknown, possibly because (1) the inaccurate modal age related to the assumption of homogeneous distribution of ^{26}Al in the protoplanetary disk, and/or (2) the six possibly contaminated ureilite samples, which have been discussed in previous work (Van Kooten et al. 2017).

Finally, our old Mn–Cr age agrees with the Mn–Cr age of the main group ureilite clasts and Hughes type clasts (representing cumulates) in a polymict ureilite (4567.9 ± 0.8 Ma), which should have similar origin to main group ureilites as they share similar ε^{54}Cr values (Van Kooten et al. 2017). However, the internal isochron ages for single main group ureilite and ALM-A and other clasts in polymict ureilites are usually younger than the bulk rock isochron suggesting a secondary event in the early evolution of UPB. In the next section, we will discuss the reasons behind the age difference.

4.3. UPB Experienced an Impact Event 4∼5 Myr after solar system Formation

The age defined from the Mn–Cr bulk isochron is older than the ages dated by ^{53}Mn–^{53}Cr and ^{26}Al–^{26}Mg internal isochrons in individual ureilites. Given the ongoing debate about the ^{26}Al distribution within the protoplanetary disk (e.g., Larsen et al. 2011; Kita et al. 2013; Bollard et al. 2019), we elected to calculate absolute ages based on ^{26}Al–^{26}Mg relative to D'Orbigny (Schiller et al. 2015), which has a nucleosynthetic makeup better matched with ureilites than CAIs. Moreover, Al–Mg ages are more consistent with U–Pb ages when anchored to D'Orbigny rather than CAIs (Wimpenny et al. 2019). These ages are listed in Table 2: 4562.7 ± 0.3 Ma (^{26}Al–^{26}Mg) and 4563.1 ± 0.5 Ma (^{53}Mn–^{53}Cr) for feldspathic clasts in a polymict ureilite (Goodrich et al. 2010), 4563.4 ± 0.3 Ma (^{26}Al–^{26}Mg) for clasts in a polymict ureilite (Kita et al. 2003), 4564.0 ± 2.2 Ma (^{53}Mn–^{53}Cr) for feldspathic clasts in a polymict ureilite (Van Kooten et al. 2017), 4563.1 ± 1.9 Ma (^{53}Mn–^{53}Cr) for clasts in Almahata Sitta (Qin et al. 2010b), 4562.0 ± 0.9 Ma (^{26}Al–^{26}Mg) and 4562.0 ± 3.4 Ma (U–Pb) for ALM-A (Bischoff et al. 2014; Amelin et al. 2015), and 4563.6 ± 0.7 Ma (^{53}Mn–^{53}Cr) for a main group ureilite (Yamakawa et al. 2010). Since the internal isochrons should date a late isotopic closure in a single rock

(i.e., Zhu et al. 2019a, 2019b), the younger ages recorded in the internal isochrons can potentially record two kinds of events for the UPB, namely the magmatic activity on the UPB that lasted 4∼5 Myr after its formation or, alternatively, a later thermal event on UPB that reset the isotopic decay systems (e.g., impact).

Magmatic processes play major roles in the formation and differentiation of planetary bodies in the solar system. A possibility is that the age differences between bulk and internal isochrons for the ureilites could potentially reflect the cooling history for the partial melts on the UPB, similar to the APB's evolution (Zhu et al. 2019b). However, there are two major weaknesses for this scenario. Polymict ureilites formed at the surface of ureilite daughter body (Goodrich et al. 2004, 2015), and there was no magma ocean on the UPB. This suggests the limited heat produced by the UPB failed to support magmatic activity on its surface for 4∼5 Myr, followed by rapid cooling. More importantly, the presence of ε^{54}Cr heterogeneity in feldspathic clasts, which can represent the melt composition, is not predicted to remain in the scenario of a prolonged magmatic activity. Since the prolonged magmatic history is unlikely, we explore another scenario accounting for the event that happened 4 Ma after the accretion of UPB.

A catastrophic disruption induced by a giant impact is believed to have occurred on UPB, because the main group ureilites (plus Almahata Sitta) usually show petrologic evidence of extremely rapid cooling (approximately 1∼20°C hr^{-1}), accompanied by a drop in pressure, through the range 1100∼650 °C (Miyamoto et al. 1985; Mittlefehldt et al. 1998; Herrin et al. 2010). This impact can effectively cause a thermal pause to reset the isotopic dating systems for the ureilites located at the surface or subsurface on UPB, which also cause the Zn evaporation (Moynier et al. 2010; Brugier et al. 2019). Moreover, the rapid melting and cooling can also cause the large ε^{54}Cr variations between individual clasts of polymict ureilites (Van Kooten et al. 2017), and maybe also the heterogeneous Δ^{17}O in Almahata Sitta (Rumble et al. 2010; Bischoff et al. 2014). In this case, the young ages recorded by the internal isochrons should represent the cooling after the impact event. However, this impact did not result in a global melting, or else the old age for the bulk main group ureilites would also have been reset. As discussed before, the disruption for UPB can be caused by this impact (Goodrich et al. 2004, 2015; Nabiei et al. 2018).

5. Conclusion

New high-precision Cr isotopic data better constrain the origin of the UPB as follows:

1. ε^{54}Cr heterogeneities between main group ureilites suggest that the UPB did not experience a global-scale process to homogenize the isotopic characteristics of the precursors in full agreement with O isotopes.
2. This heterogeneity may result from a mixing process between two reservoirs; one that possesses high Mn/Cr, high ε^{54}Cr, high Mg#, low Fe/Mn, low Δ^{17}O, and low δ^{13}C, with another one having low Mn/Cr, ε^{54}Cr, and Mg#, and high Fe/Mn, Δ^{17}O, and δ^{13}C.
3. The ^{55}Mn/^{52}Cr correlates well with ε^{53}Cr among main group ureilites. An external ^{53}Mn–^{53}Cr isochron aged at 4566.7 ± 1.5 Ma can be established. This old age likely reflects a combination of the existence of primordial differences in Mn/Cr ratios in the ureilite precursors and an early partial melting process occur within the first 1 Ma in the solar system.
4. The ages dated by individual clasts in polymict ureilites postdates the UPB's accretion by 4∼5 Myr, which suggests these are resetting ages arising from an impact event that causing the melting and quenching.

F.M. acknowledges funding from the European Research Council under the H2020 framework program/ERC grant agreement (#637503-Pristine) and financial support of the UnivEarthS Labex program at Sorbonne Paris Cité (#ANR-10-LABX-0023 and #ANR-11-IDEX-0005-02), and the ANR through a chaire d'excellence Sorbonne Paris Cité. M.B. acknowledges funding from the Danish National Research Foundation (#DNRF97) and the European Research Council (#616027-Stardust2Asteroids). We are deeply appreciative of the detailed and insightful comments by Cyrena A. Goodrich, which greatly improved the quality of this paper, and efficient editorial handling by AAS scientific editor, Faith Vilas. K.Z. thanks the China Scholarship Council for a PhD fellowship (#201706340161) and O. Richard Norton Award (travel grant) and Wiley Award (outstanding oral presentation award) from The Meteoritical Society to present this work on MetSoc 2019.

ORCID iDs

Ke Zhu (朱柯) https://orcid.org/0000-0003-3613-7239

References

Amelin, Y. 2008, GeCoA, 72, 221
Amelin, Y., Koefoed, P., Bischoff, A., et al. 2015, in 78th Annual Meeting of the Meteoritical Society, 1856, 5344
Baker, J. A., Schiller, M., & Bizzarro, M. 2012, GeCoA, 77, 415
Barrat, J.-A., Jambon, A., Yamaguchi, A., et al. 2016, GeCoA, 194, 163
Barrat, J.-A., Rouxel, O., Wang, K., et al. 2015, E&PSL, 419, 93
Barrat, J.-A., Sansjofre, P., Yamaguchi, A., Greenwood, R. C., & Gillet, P. 2017, E&PSL, 478, 143
Bischoff, A., Horstmann, M., Barrat, J.-A., et al. 2014, PNAS, 111, 12689
Bizzarro, M., Connelly, J. N., & Krot, A. N. 2017, Chondrules: Ubiquitous Chondritic Solids Tracking the Evolution of the Solar Protoplanetary Disk, Formation, Evolution, and Dynamics of Young Solar Systems (Berlin: Springer), 161
Bizzarro, M., Paton, C., Larsen, K., et al. 2011, Journal of Analytical Atomic Spectrometry, 26, 565
Bollard, J., Connelly, J. N., Whitehouse, M. J., et al. 2017, SciA, 3, e1700407
Bollard, J., Kawasaki, N., Sakamoto, N., et al. 2019, GeCoA, 260, 62
Bonnand, P., & Halliday, A. N. 2018, NatGe, 11, 401
Brearley, A. J. 1992, GeCoA, 56, 1373
Brennecka, G. A., & Wadhwa, M. 2012, PNAS, 109, 9299
Broadley, M. W., Bekaert, D. V., Marty, B., Yamaguchi, A., & Barrat, J. A. 2019, GeCoA, 270, 325
Brugier, Y.-A., Barrat, J.-A., Gueguen, B., et al. 2019, GeCoA, 246, 450
Budde, G., Kruijer, T. S., Fischer-Gödde, M., Irving, A. J., & Kleine, T. 2015, E&PSL, 430, 316
Chen, H.-W., Lee, T., Lee, D.-C., Jiun-San Shen, J., & Chen, J.-C. 2011, ApJL, 743, L23
Clayton, R. N., & Mayeda, T. K. 1988, GeCoA, 52, 1313
Clayton, R. N., & Mayeda, T. K. 1996, GeCoA, 60, 1999
Cohen, B. A., Goodrich, C. A., & Keil, K. 2004, GeCoA, 68, 4249
Connelly, J. N., Bizzarro, M., Krot, A. N., et al. 2012, Sci, 338, 651
Dauphas, N., Remusat, L., Chen, J., et al. 2010, ApJ, 720, 1577
Downes, H., Mittlefehldt, D. W., Kita, N. T., & Valley, J. W. 2008, GeCoA, 72, 4825
Eugster, O. 2003, ChEG, 63, 3
Glavin, D., Kubny, A., Jagoutz, E., & Lugmair, G. 2004, M&PS, 39, 693
Goodrich, C., Treiman, A., & Boyle, S. 2017, LPSC, 48, 1196
Goodrich, C. A. 1992, Metic, 27, 327
Goodrich, C. A. 1999, M&PS, 34, 109
Goodrich, C. A., & Delaney, J. S. 2000, GeCoA, 64, 149
Goodrich, C. A., Hartmann, W. K., O'Brien, D. P., et al. 2015, M&PS, 50, 782

Goodrich, C. A., Hutcheon, I. D., Kita, N. T., et al. 2010, E&PSL, 295, 531
Goodrich, C. A., Patchett, P. J., Lugmair, G. W., & Drake, M. J. 1991, GeCoA, 55, 829
Goodrich, C. A., Scott, E. R., & Fioretti, A. M. 2004, ChEG, 64, 283
Goodrich, C. A., Van Orman, J. A., & Wilson, L. 2007, GeCoA, 71, 2876
Göpel, C., Birck, J.-L., Galy, A., Barrat, J.-A., & Zanda, B. 2015, GeCoA, 156, 1
Greenwood, R. C., Burbine, T. H., Miller, M. F., & Franchi, I. A. 2017, ChEG, 77, 1
Greenwood, R. C., Franchi, I., Jambon, A., Barrat, J.-A., & Burbine, T. 2006, Sci, 313, 1763
Greenwood, R. C., Franchi, I. A., Jambon, A., & Buchanan, P. C. 2005, Natur, 435, 916
Herrin, J. S., Zolensky, M. E., Ito, M., et al. 2010, M&PS, 45, 1789
Holden, N. E. 1990, PApCh, 62, 941
Ikeda, Y. 2007, PolSc, 1, 45
Inglis, E. C., Creech, J. B., Deng, Z., & Moynier, F. 2018, ChGeo, 493, 544
Johansen, A., Low, M.-M. M., Lacerda, P., & Bizzarro, M. 2015, SciA, 1, 1500109
Kita, N., Ikeda, Y., Shimoda, H., Morishita, Y., & Togashi, S. 2003, LPSC, 34, 1557
Kita, N. T., Ikeda, Y., Togashi, S., et al. 2004, GeCoA, 68, 4213
Kita, N. T., Yin, Q. Z., MacPherson, G. J., et al. 2013, M&PS, 48, 1383
Larsen, K. K., Trinquier, A., Paton, C., et al. 2011, ApJL, 735, L37
Larsen, K. K., Wielandt, D., & Bizzarro, M. 2018, Journal of Analytical Atomic Spectrometry, 33, 613
Larsen, K. K., Wielandt, D., Schiller, M., & Bizzarro, M. 2016, Journal of Chromatography A, 1443, 162
Li, S., Yin, Q.-Z., Bao, H., et al. 2018, GeCoA, 242, 82
Liu, J., Qin, L., Xia, J., et al. 2019, GeCoA, 251, 73
Lodders, K. 2003, ApJ, 591, 1220
Lugmair, G., & Shukolyukov, A. 1998, GeCoA, 62, 2863
McDonough, W. F., & Sun, S.-S. 1995, ChGeo, 120, 223
Mittlefehldt, D. W., McCoy, T. J., Goodrich, C. A., & Kracher, A. 1998, RvMG, 36, 1
Miyamoto, M., Takeda, H., & Toyoda, H. 1985, JGRB, 90, 116
Mougel, B., Moynier, F., & Göpel, C. 2018, E&PSL, 481, 1
Moynier, F., Beck, P., Yin, Q.-Z., et al. 2010, ChGeo, 276, 374
Moynier, F., Yin, Q.-Z., & Jacobsen, B. 2007, ApJL, 671, L181
Nabiei, F., Badro, J., Dennenwaldt, T., et al. 2018, NatCo, 9, 1327
Nittler, L. R., Alexander, C. M. D., Liu, N., & Wang, J. 2018, ApJL, 856, L24
Pedersen, S. G., Schiller, M., Connelly, J. N., & Bizzarro, M. 2019, M&PS, 54, 1215
Petitat, M., Birck, J.-L., Luu, T., & Gounelle, M. 2011, ApJ, 736, 23
Qin, L., Alexander, C. M. O. D., Carlson, R. W., Horan, M. F., & Yokoyama, T. 2010a, GeCoA, 74, 1122
Qin, L., Nittler, L. R., Alexander, C. M. O. D., et al. 2011, GeCoA, 75, 629
Qin, L., Rumble, L., Alexander, C. M. O. D, et al. 2010b, M&PS, 45, 1771
Rai, V. K., Murty, S. V. S., & Ott, U. 2003, GeCoA, 67, 4435
Rankenburg, K., Humayun, M., Brandon, A., & Herrin, J. 2008, GeCoA, 72, 4642
Rumble, D., Zolensky, M. E., Friedrich, J. M., Jenniskens, P., & Shaddad, M. H. 2010, M&PS, 45, 1765
Sanders, I. S., Scott, E. R. D., & Delaney, J. S. 2017, M&PS, 52, 690
Schiller, M., Bizzarro, M., & Fernandes, V. A. 2018, Natur, 555, 507
Schiller, M., Connelly, J. N., Glad, A. C., Mikouchi, T., & Bizzarro, M. 2015, E&PSL, 420, 45
Schiller, M., Van Kooten, E., Holst, J. C., Olsen, M. B., & Bizzarro, M. 2014, Journal of Analytical Atomic Spectrometry, 29, 1406
Shima, M., & Honda, M. 1966, E&PSL, 1, 65
Shukolyukov, A., & Lugmair, G. 2006, E&PSL, 250, 200
Singletary, S. J., & Grove, T. L. 2003, M&PS, 38, 95
Skirdji, M., & Warren, P. 2001, M&PSA, 36, A189
Sossi, P., Moynier, F., & van Zuilen, K. 2018, PNAS, 115, 10920
Sossi, P. A., Klemme, S., O'Neill, H. S. C., Berndt, J., & Moynier, F. 2019, GeCoA, 260, 204
Torigoye-Kita, N., Misawa, K., & Tatsumoto, M. 1995a, GeCoA, 59, 381
Torigoye-Kita, N., Tatsumoto, M., Meeker, G. P., & Yanai, K. 1995b, GeCoA, 59, 2319
Trinquier, A., Birck, J.-L., & Allègre, C. J. 2007, ApJ, 655, 1179
Trinquier, A., Birck, J.-L., & Allègre, C. J. 2008a, Journal of Analytical Atomic Spectrometry, 23, 1565
Trinquier, A., Birck, J. L., Allègre, C. J., Göpel, C., & Ulfbeck, D. 2008b, GeCoA, 72, 5146
Trinquier, A., Elliott, T., Ulfbeck, D., et al. 2009, Sci, 324, 374
Van Kooten, E. M. M. E., Schiller, M., & Bizzarro, M. 2017, GeCoA, 208, 1
Van Kooten, E. M. M. E., Wielandt, D., Schiller, M., et al. 2016, PNAS, 113, 2011
Vermeesch, P. 2018, Geoscience Frontiers, 9, 1479
Warren, P. H. 2011, GeCoA, 75, 6912
Warren, P. H. 2012, M&PS, 47, 209
Warren, P. H., & Huber, H. 2006, M&PS, 41, 835
Warren, P. H., Ulff-Møller, F., Huber, H., & Kallemeyn, G. W. 2006, GeCoA, 70, 2104
Weidenschilling, S. 2011, Icar, 214, 671
Wilson, L., Goodrich, C. A., & Van Orman, J. A. 2008, GeCoA, 72, 6154
Wimpenny, J., Sanborn, M. E., Koefoed, P., et al. 2019, GeCoA, 244, 478
Yamakawa, A., Yamashita, K., Makishima, A., & Nakamura, E. 2010, ApJ, 720, 150
Yamakawa, A., & Yin, Q.-Z. 2014, M&PS, 49, 2118
Yamashita, K., Maruyama, S., Yamakawa, A., & Nakamura, E. 2010, ApJ, 723, 20
Zhang, J., Dauphas, N., Davis, A. M., Leya, I., & Fedkin, A. 2012, NatGe, 5, 251
Zhu, K., Liu, J., Moynier, F., et al. 2019a, ApJ, 873, 82
Zhu, K., Moynier, F., Barrat, J.-A., et al. 2019b, ApJL, 877, L13
Zhu, K., Sossi, P. A., Siebert, J., & Moynier, F. 2019c, GeCoA, 266, 598